Title

High-density Neural Recordings from Feline Sacral Dorsal Root Ganglia with Thin-film Array

Authors

Zachariah J. Sperry[1,2], Kyounghwan Na[3], James Jun[4], Lauren R. Madden[1,2], Alec Socha[2,3], Eusik Yoon[1,3,5], John P. Seymour[1,3,6,7], Tim M. Bruns[1,2,*]

Author Affiliations

1. Biomedical Engineering, University of Michigan, Ann Arbor, MI, USA
2. Biointerfaces Institute, University of Michigan, Ann Arbor, MI, USA
3. Electrical Engineering and Computer Science, University of Michigan, Ann Arbor, MI, USA
4. Flatiron Institute, Simons Foundation, New York City, NY, USA
5. Center for Nanomedicine, Institute for Basic Science (IBS) and Graduate Program of Nano Biomedical Engineering (NanoBME), Advanced Science Institute, Yonsei University, Seoul, Korea.
6. Department of Neurosurgery, University of Texas Health Science Center, Houston, TX, USA
7. Department of Electrical and Computer Engineering, Rice University, Houston, TX, USA

*Corresponding author

Contact info

Dr. Tim Bruns, bruns@umich.edu

Abstract

Objective: Dorsal root ganglia (DRG) are promising sites for recording sensory activity. Current technologies for DRG recording are stiff and typically do not have sufficient site density for high-fidelity neural data techniques. Approach: We demonstrate neural recordings in sacral DRG of anesthetized felines using a 4.5 µm-thick, high-density flexible polyimide microelectrode array with 60 sites and 30-40 µm site spacing. We delivered arrays into DRG with ultrananocrystalline diamond shuttles designed for high stiffness affording a smaller footprint. We recorded neural activity during sensory activation, including cutaneous brushing and bladder filling. We used a specialized neural signal analysis software to sort densely-packed neural signals. Main results: We successfully delivered arrays in five of six experiments and recorded sensory activity in four experiments. The median neural signal amplitude was 55 µV peak-to-peak and the maximum unique units recorded at one array position was 260, with 157 driven by sensory or electrical stimulation. In one experiment, we used the neural analysis software to track eight signals as the array was retracted ~500 µm. Significance: This study is the first demonstration of ultrathin, flexible, high-density electronics delivered into DRG, with capabilities for recording and tracking sensory information that are a significant improvement over conventional DRG interfaces.

Keywords: DRG, dorsal root ganglia, microelectrode, polyimide, spike sorting

Introduction

Dorsal root ganglia (DRG) are neural structures with tremendous potential as bioelectrical interface sites, but current technologies available to access, map, and utilize the dense sensory information they contain are limited. As peripheral nerves enter the central nervous system, sensory neurons first coalesce at each spinal level into bilateral dorsal spinal nerves. These nerves, or dorsal roots, each contain a single ganglion, or DRG, which in turn contain the unmyelinated cell bodies of all sensory neurons entering that spinal level. When conducting an action potential, these cell bodies generate a relatively large extracellular potential detectable at single-unit fidelity by nearby recording electrodes [1]. The sensory information that can be decoded from these signals can be used as feedback to control, for example, neural stimulation for bladder control or walking [2]–[7].

However, much remains unknown about the intrinsic anatomy of DRG. Previous studies have presented some evidence of functional organization within individual DRG [8], [9], but the overall structure-function relationship still remains unclear. In comparison, functional organization relationships in the brain and spinal cord have been well-characterized, possibly allowing for the development of selectively targeted neural interfaces for particular applications. Presently DRG can be targeted to choose a ganglion at a particular spinal level, such as sacral DRG for bladder-related applications or lumbar DRG for lower limb neuroprostheses. Within-DRG interfacing for selective access to individual peripheral nerve pathways generally depends on the random nature of inserted microelectrodes being located near axons of interest, however. Tools to study the organization of DRG *in vivo* could lead to more selective targeting within these structures.

The current standard for *in vivo* recording of DRG neurons is the Utah array, a commercially available, silicon-based, penetrating microelectrode array. Previous studies have successfully demonstrated the capability of Utah arrays to record a variety of sensory neurons in the DRG, including populations related to urinary tract function, joint flexion, and skin sensation [2]–[7]. However, the mechanical mismatch between silicon and neural tissue causes tissue damage and scarring *in vivo* [10]. Additionally, from a neural mapping perspective, a Utah array shank is only capable of recording from a single depth at a given location in the DRG, with a site spacing of no less than 400 µm. Floating microelectrode arrays (FMAs), which allow for custom shank lengths and tip impedances, have been used for DRG recording and stimulation with a minimum 250 µm site spacing [11]–[14], and also

have scarring around electrode shanks for chronic *in vivo* implants [15]. Both Utah arrays and FMAs are unable to track neurons that shift away from electrode sites, such as due to electrode micromotion or scar tissue buildup. The smallest site spacing reported as used in DRG was a stiff single-shank silicon probe with 50 µm electrode-site spacing (a "Michigan probe") [16]. While a Michigan probe may track vertical shifts in neuron position, a smaller electrode site spacing would allow for over-sampling of neurons. Furthermore, the stiff nature of these probes will also have a chronic tissue-scarring response as has been reported in the brain [17]. An ideal mapping technology would have a reduced stiffness and be able to record from multiple depths at multiple locations to maximize the number of sampled neurons.

Based on these constraints, a flexible and high-density electrode array would be the preferred interface for mapping within DRG. One way to achieve this is with planar electrode arrays with a thin-film polymer substrate, first described for high-fidelity neural recording in the brain by Rousche et al. (2001) [18]. We previously reported the use of a high-density non-penetrating polyimide array for single-unit neural recording from the surface of lumbosacral DRG [19], and studies have used other technologies to record from the DRG surface, [20]–[22] but biophysical limitations suggest that no units would be recorded below about 200 µm below the surface. Though anatomical analysis suggests that the highest density of somata reside in this outer dorsal region of the DRG [23], [24], selective mapping or microstimulation requires a technology interfacing with the interior of DRG.

In this study, we demonstrate high-density recording and mapping applications in sacral feline DRG using a flexible polymer array developed by Na et al. at the University of Michigan [25]. The array was similar in design to the one reported in Sperry et al. (2017) [19], but was delivered into the DRG with a novel structurally-stiffened diamond shuttle. Sacral DRG were targeted because of their potential use as interface sites for bladder neuroprosthetic devices, though the technology could be directly transferred to other spinal levels or neural interface sites. We successfully delivered arrays in 5/6 experiments and recorded high-density sensory neural activity in 4 of these experiments. We used this high-density information to efficiently sort the neural signals and to track individual neurons as the array was moved through the DRG to simulate the extremes of chronic recording conditions.

Methods

Microelectrode Array

The primary purpose of this study was to explore the recording and mapping capabilities of a high-density microelectrode array in feline sacral DRG. Arrays were fabricated in the Lurie Nanofabrication facility utilizing the same process described for the ganglionic surface electrode arrays in Sperry et al. 2018 [19], but with modifications in the overall design. In brief, platinum electrode sites were patterned and connected with gold/platinum traces sandwiched in the middle of a 4.5 µm thick flexible polyimide substrate. In this study, each of the 60 sites were approximately square, with an area of 400 μm^2, and arranged in 2 off-set columns. The pitch between electrodes was 40 µm. The active portion of the array was 1160 µm long and tapered from 80 µm wide to 55-µm wide for most of the length of the shank. Figure 1(a) shows a schematic of the array.

Each array was bonded to a custom printed circuit board (PCB) for interfacing with the neural recording system. To reduce site impedance prior to recording, array channels were coated with poly(3,4-ethylenedioxythiophene) polystyrene sulfonate (PEDOT:pSS) as described in Patel et al., with the current adjusted for the electrode site area [47]. To verify all deposition and coating steps, impedance measurements were taken with a PGSTAT12 Autolab (EcoChemie, Utrecht, Netherlands), controlled by vendor supplied NOVA software. Measurements were obtained by applying a 1 kHz 10 mV_{rms} signal. Custom MATLAB (Mathworks, Natick, MA) scripts were used to determine frequency-specific impedance

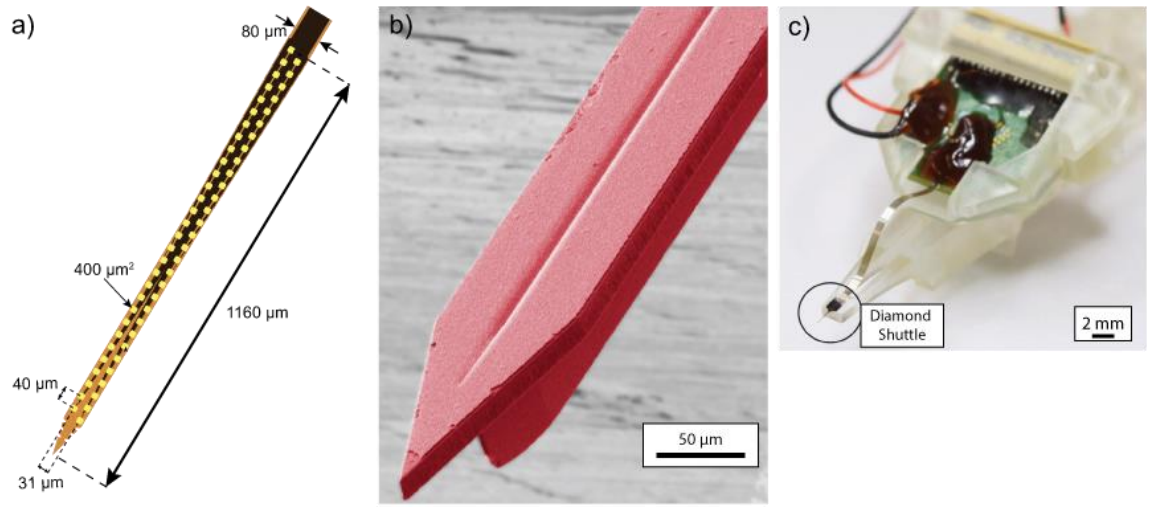

Figure 1: Flexible intraneural DRG array. (a) Tip of flexible high-density array showing locations of 60 electrode sites (yellow) and dimensions. (b) Diamond shuttle imaged with electron microscope, false color for visibility. (c) Insertion jig, with location of diamond shuttle highlighted in a circle.

values. The PCB board was placed in a custom 3D-printed jacket and mounted to a 3D-printed insertion jig (Form2 3D printer, Formlabs, Somerville, MA) (Figure 1(c)).

For delivery into DRG, the flexible array was temporarily adhered to an ultrananocrystalline diamond (UNCD) shuttle with water-soluble polyethylene glycol (PEG; 12,000 MW) or ultraviolet-cured cyanoacrylate glue. The shuttle was fabricated with a stiffened T-profile by UNCD deposition over a trench which was etched away to form the final shape (fabrication details and characterization in Na et al. 2020) [25]. The shuttle was 65 µm wide, with a planar 11 µm thickness. The T-profile extended 27.5 µm from the back with a width diminishing from 16 µm to 2 µm. This material and profile increased the buckling load of the shuttle by a factor of 13 as compared to a planar silicon shuttle without the T-stiffened profile [25]. This design allowed for array insertion without removal of the tough epineural layer surrounding the DRG, but with presumably less damage to the surrounding tissue. A colorized close-up of the shuttle is shown in Figure 1 (b). The shuttle was glued to the end of the insertion jig prior to adhering the array. The combined array, PCB, jacket, shuttle, and insertion jig will be collectively referred to as the insertion assembly. Figure 1 (c) shows the insertion jig close-up.

In Vivo Deployment and Neural Recording

Neural recordings were performed in the DRG of intact, domestic, short-haired adult cats (Liberty Research, Inc., Waverly, NY). All procedures were approved by the University of Michigan Institutional Animal Care and Use Committee, in accordance with the National Institute of Health's guidelines for the care and use of laboratory animals. Animals were free-range housed prior to use with 0–3 other male cats in a 413 ft^2 room with controlled temperature (19 °C–21 °C) and relative humidity (35%–60%), food and water available ad lib, a 12 h light/dark cycle, and enrichment via toys and daily staff interaction.

Initial anesthesia was induced with an intramuscular dose of ketamine (6.6 mg kg^{-1})-butorphanol (0.66 mg kg^{-1})-dexmedetomidine (0.033 mg kg^{-1}) intramuscular (IM) dose. Animals were intubated, then maintained on isoflurane anesthesia (2%–4%) during the remainder of the procedure. Respiratory rate, heart rate, end-tidal CO_2, O_2 perfusion, temperature, and intra-arterial blood pressure were monitored continuously using a Surgivet vitals monitor (Smiths Medical, Dublin, OH). Intravenous (IV) lines were inserted into one or both cephalic veins for infusion of drugs and intravenous fluids (1:1 ratio of lactated Ringers solution and 5% dextrose, 5–30 ml kg^{-1} h^{-1}).

A laminectomy (removal of dorsal spinal column bone) was performed to expose the lumbosacral spinal cord and sacral DRG (typically S1–S2). Following laminectomy, the cat's pelvis was suspended from a custom support frame (80/20 Inc., Columbia City, IN) with stainless steel wire and bilateral bone screws in the superior posterior pelvic crest to minimize spinal motion during breathing and bladder filling. A separate stabilizing frame consisting of optomechanical components (Thor Lab, Newton, New Jersey) and custom 3D-printed components was assembled around the animal to support a 3-axis micromanipulator (502600, World Precision Instruments, Sarasota, FL) and linear actuator (M-235.5DD, Physik Instrumente, Karlsruhe, Germany). The insertion assembly was mounted to the end of the linear actuator, aimed at either the S1 or S2 DRG, and inserted at 2 mm s^{-1}. Insertion was monitored with a USB microscope camera.

The reference wire (and ground wire, when not shorted to the reference on the PCB) was connected to a 12-gauge stainless steel needle inserted under the skin on the flank. Neural activity was recorded at 30 kHz using the Ripple Grapevine Neural Interface Processor and associated Trellis software (Ripple Neuro, Salt Lake City, UT). We simultaneously monitored bladder pressure at 1 kHz through the urethral catheter with a pressure transducer (DPT-100, Utah Medical Products, Midvale, UT) and analog amplifier (SYS-TBM4M, World Precision Instruments, Sarasota, FL).

A variety of sensory stimuli were applied to activate sacral afferent neurons, to map the location of different neuronal types along the array and to demonstrate the array's potential usefulness for neural prosthesis research. To activate skin afferents, the skin was brushed using a cotton applicator in the sacral dermatome associated with the DRG of interest, including regions of the tail, the anus, the perineum, the external meatus of the penis, and the scrotum [30], [48]. These trials typically involved brushing in bouts of 10 s with 10 s rest periods between bouts. Visceral afferents of the urethra were activated by sliding a catheter back and forth in the orifice. To activate bladder afferents, room-temperature saline was infused through the urethral catheter in sequential boluses of 10 mL each.

For measurements of nerve conduction velocity (CV), electrical stimulation was applied (biphasic, 1:2 charge balanced, cathode-leading, 200 µs pulse-width) at low levels (15–300 µA) to the ipsilateral pudendal nerve via an implanted bipolar nerve cuff (2.0 mm inner diameter Silastic 508-009 tubing; 0.4 mm stainless steel Cooner wire contacts [10]). As an

alternative stimulation site, a pair of fine-wire electrodes (stainless steel, 50 µm diameter, Model EMT-2-30, Microprobes, Gaithersburg, MD) was inserted near the anal sphincter and stimulated with a similar waveform at a higher amplitude to generate muscle twitch (0.3-4mA).

At the end of each experiment, euthanasia was achieved with an intravenous dose of sodium pentobarbital (390 mg ml^{-1}) under deep isoflurane anesthesia, followed by bilateral pneumothorax. To add context to recordings, DRG from some experiments were removed and fixed in formalin, processed into parafinn blocks, stained with hematoxylin and eosion, and imaged with an inverted microscope (IX83, Olympus, Shinjuku, Tokyo City, Tokyo, Japan), with the brightfield setting at 10 times magnification and Nikon (Minato, Tokyo City, Tokyo, Japan) Element BR 3.2 Software.

Data Analysis

In order to efficiently handle the large data sets generated by these recordings, we chose to use the open source IronClust suite for MATLAB, which is specifically optimized for high-density probes that oversample individual neurons [41]. Our spike-sorting workflow using IronClust (developed by James Jun and teams at the Janelia Research Campus and the Flatiron Institute) consists of 1) preprocessing, 2) spike detection & feature extraction, 3) density-graph clustering, and 4) manual clustering. We chose IronClust for its real-time processing speed with a GPU and its ability to accurately handle the potential probe drift on flexible probes. Each recorded channel was band-pass filtered (300-6000 Hz) and the narrow-band noise peaks were automatically removed in the frequency domain if they exceeded 10 MAD (median absolute deviation) above the median trend curve. Subsequently, the common-mode noise was removed by subtracting each channel by the average across all channels. The remaining motion artifact primarily due to analog-to-digital conversion saturation was rejected by computing the standard deviation of the filtered signals across all channels in each time bin (5 ms duration), and the spike detection was disabled in the time bins exceeding a MAD threshold of 20. The spikes were detected at their negative peaks exceeding 5 MAD threshold [49], and duplicate spikes from the same and neighboring channels were removed if larger peaks were detected within their spatiotemporal neighborhood (50 µm, 0.3 ms). Spike waveforms (1 ms width) surrounding each peak event are extracted from a fixed number of adjacent channels (80 µm). For each spike, we also extracted spike waveforms centered at its secondary peak channel to account

for the random jitters of the peak channel due to recording noise and probe drift. Two principal component features were extracted from each channel using a common set of principal vectors for all channels.

In order to handle the probe drift, time bins where the probe occupied similar anatomical locations were grouped together based on the similarity of the 2D histogram of the spike amplitudes and positions. Anatomical snapshots were computed at regular spike-count intervals such that each snapshot contains an equal number of spike events from all channels (20 s average duration). For each snapshot, a 2D histogram representing the anatomical features was computed by counting spikes based on their amplitude quantiles (8 bins) and center-of-mass positions on the probe. Each time bin was grouped with 14 other time bins exhibiting high similarity scores to form a 300 s average duration. *k*-nearest neighbor (k_{NN}, k=30) distances (d_{knn}) were computed between spikes whose peak appeared in channel *c* and time bin *s* with the neighboring spikes whose peak or second peak appeared in channel *c* and time bins that were anatomically grouped with *s*.

Density-graph clustering was performed based on the k_{NN} [50], [51] by considering a fixed number of local neighbors to achieve a linear scaling. For each spike *j*, the local density score was calculated ($\rho_j = 1/d_{knn,j}$), and the distance separation score ($\boldsymbol{\delta}_j = d_{min,j} / d_{knn,j}$) was calculated where $d_{min,j}$ is the distance in the principal component feature space to the nearest spike k having a greater density score ($\min(dj_k \mid \rho_k > \rho_j)$). Local density peak points were identified based on a density separation criterion ($\boldsymbol{\delta} > 1$) and the cluster memberships were recursively assigned to the nearest points toward a decreasing density gradient. To minimize false splitting errors due to drift or bursting, units exhibiting similar waveform shapes were merged (Pearson correlation > 0.985). Finally, clusters were manually split, merged, or deleted by using a set of multiple interactive views in the MATLAB-based GUI.

To understand the relationship between sensory inputs and neural activity, we calculated the correlation of either bladder pressure or cutaneous brushing (coded as a continuous binary on/off signal). We used a correlation threshold of >0.4 for bladder pressure or >0.6 for cutaneous brushing to identify related units. In a small number of bladder pressure trials, there was a clear visual relationship between the bladder pressure and the firing rate which did not yield a high correlation, and these units were also included. The signal to noise ratio (SNR) was defined as the unit peak-to-peak amplitude divided by the root mean square voltage of the channel during the entire trial.

For trials with electrical stimulation, a post-stimulus time histogram (PSTH) was generated for each detected unit. If a firing unit had stimulus-locked timing, we used a normal distribution fitted to the PSTH to determine the mean and standard deviation of the delay. To calculate conduction velocity (CV), we assumed a pudendal nerve to sacral DRG length of 9 cm and an anal sphincter to sacral DRG length of 12 cm based on previous measurements [10].

Results

In this study we recorded high numbers of sensory neurons from feline sacral DRG, identifying single-unit activity from a range of stimuli. The high-density array layout allowed for oversampling of units across electrode sites for enhanced sorting capabilities and tracking of units while the array was retracted. The thin-film polyimide array shown in Figure 1(a) was introduced into DRG adhered to an ultrananocrystalline diamond shuttle with a T-shaped profile, shown in Figure 1(b). A 3D-printed insertion jig, pictured in Figure 1(c) allowed the array, shuttle, and electronics to be mounted and delivered into DRG using a linear insertion motor. The physical range of channels, physical range of units, number of units, peak-to-peak amplitude, and signal-to-noise ratio (SNR) are reported in Table 1.

The median peak-to-peak amplitude of recorded units was typically on the order of 50-60 µV, though the maximum observed cluster center had an amplitude of 1334 µV (a tonically activated unit in experiment 3 with 2.2 ± 0.48 Hz firing rate, modulated to ~3 Hz by anus brushing). The minimum observed single-unit cluster center with sensory correlation had a mean amplitude of 20.5 µV and SNR of 4.21 (bladder-pressure modulated unit in experiment 2, correlation 0.64). This was an example of neural activity that might not have been detected using traditional neural unit sorting on individual channels. Other multi-unit activity was observed with smaller mean amplitude, but the unit shapes were poorly correlated. Bladder pressure related units were observed in 2 of the experiments. An example bladder unit is shown in Figure 2 (a), with the waveforms at the five highest amplitude channels shown on the right. Cutaneous brushing units were observed in all 4 experiments with neural activity. Units were observed with correlation to scrotal brushing, anal brushing, and brushing the dorsal base of the tail. An example unit related to tail brushing is shown in Figure 2 (b).

TABLE 1: Summary of units recorded during all 6 experiments. Number of driven units is given by unit type: cutaneous (C), bladder (B), electrical stimulation of the anal sphincter (A) or pudendal nerve (P). Number of units by trial, peak-to-peak amplitude, and SNR are given as median with interquartile (IQ) range. For experiment 2, which had three successful positions of a single insertion, select details about each position are given in rows. See Figure 3 for position reference.

Expt	**Driven Units**				**All Trial Channel Range (µm)**	**Number of Units by Trial**	**Peak-to-peak Amplitude (µV)**	**SNR**
	C	*B*	*A*	*P*		*Median (IQ Range)*		
1	2	2	0	0	300	2.5 (1.0)	61.8 (79.4)	5.0 (2.4)
2 (1)	99	13	28	17	680	27.0 (11.0)	54.6 (58.3)	5.9 (7.5)
(2)	70	34	14	21	1120	24.0 (8.0)		
(3)	42	8	6	29	860	14.5 (4.3)		
3	64	0	21	12	1080	21.5 (14.8)	52.6 (73.4)	5.7 (9.6)
4	5	0	0	0	640	6*	27.8 (38.7)	3.1 (4.2)
5	*Insertion without units*							
6	*Unsuccessful insertion*							

Units activated by electrical stimulation of the pudendal nerve or anal sphincter were observed in 2 of the experiments. There was no significant difference in the population of conduction velocities elicited by pudendal or anal stimulation. An example unit is shown in Figure 2 (c), with the associated PSTH showing a delay of 34 ± 7 ms from stimulation to recording. This unit showed a characteristic double spike response to stimulation (anal sphincter, 2 Hz, 3.2 mA), with the first peak around 27 ms and the second around 41 ms. The early peak yields a CV of about 4.4 m/s, which suggests an Aδ-type fiber [26]. There are a number of possible explanations for the second peak. The first peak is most likely a direct activation of the nerve ending by electrical stimulation, and the second likely originates as a result of an ensuing evoked muscle twitch. A variety of single and double-activated units were found in the data set. The longest delay for a directly activated unit was 203 ± 3 ms (CV: 0.44 ± .01 m/s, a pudendal activated C-fiber [26]). The shortest delay for a directly activated unit was 7 ± 0 ms (CV: 12.86 ± 0 m/s, a pudendal activated Aδ-fiber [26]). Other units had a less specific activation tied to stimulation. These units (amplitude on the order of 20-30 µV) were more likely to be active in the period 35-75 ms after a stimulus, but with delay standard deviations of up to 42 ms.

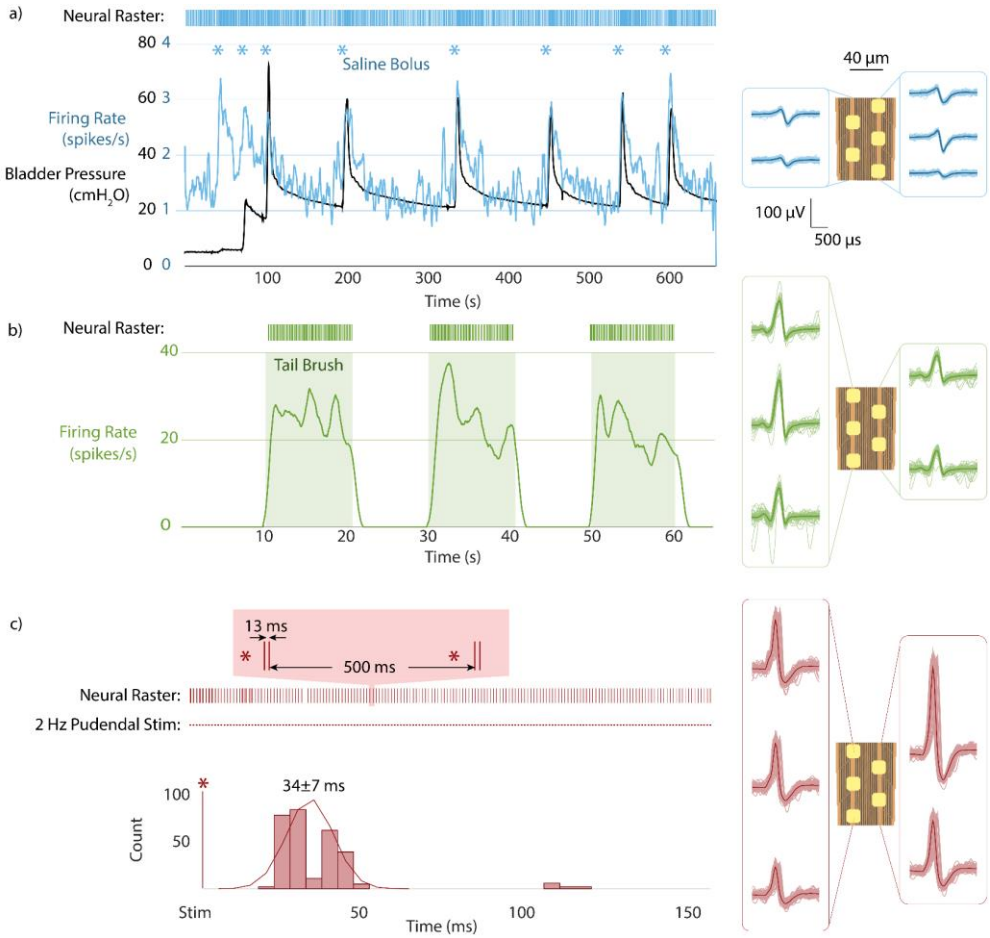

Figure 2: Sample of sensory units recorded from sacral DRG. (a) Bladder-pressure correlated unit from saline bolus fills. Firing rate shown with recorded bladder pressure. Raster plot shows actual spike times. Waveforms shown at right in relation to channels. (b) Tail-brushing correlated unit. (c) Anal sphincter electrical stimulus driven unit (2 Hz, 3.2 mA). Magnified raster plot shows characteristic double-spike response with ~27 then ~41 ms stimulus delay. PSTH shown below neural raster.

In experiment 2, neural activity was recorded with the array at 3 different positions in the DRG, with a full insertion (position 1) followed by retraction to other 2 positions in 80 µm steps (positions 2 and 3). Figure 3 (a) shows the modulated and spontaneous activity recorded at each position. Following the experiment, the DRG used was removed, fixed, sectioned axially, and stained with hematoxylin and eosin (H&E) to highlight cell locations. While the exact position of the array relative to the stained section is not known, by comparing the activated regions with the histology we can estimate the position of the array in the DRG and the ventral root (VR) below, from which we do not expect to record any sensory-evoked units. Figure 3 (b) shows the putative location of the array relative to the DRG cross section.

Figure 4 (a) shows the number of identified clusters that were detected at each electrode site for the three primary locations in Experiment 2. For these array locations,

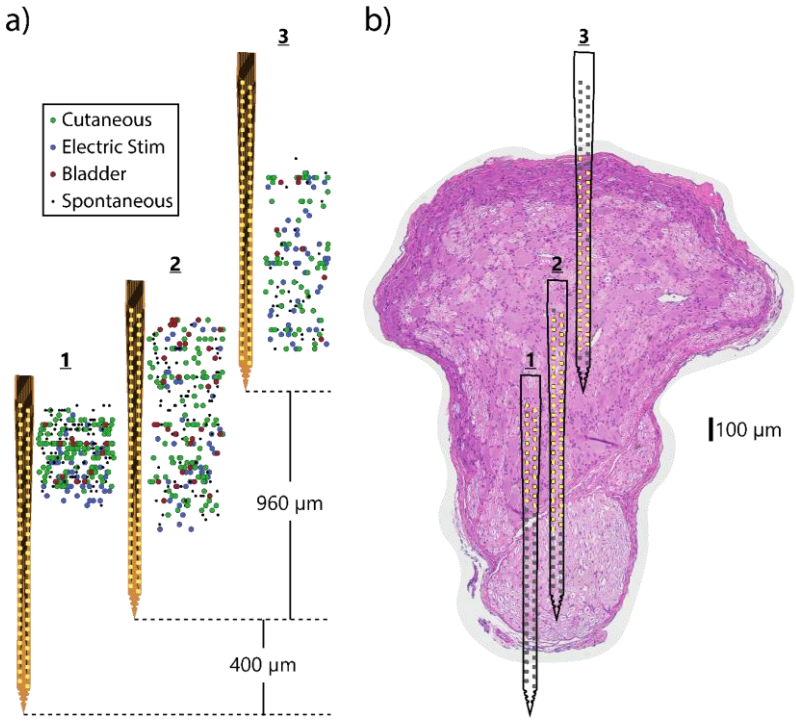

Figure 3: Summary of neural units recorded at different positions in DRG in one experiment. (a) Three different vertical positions of the array in one experiment showing the locations of recorded units (note: horizontal position is not relevant, points jittered for clarity). (b) Putative position of the array relative to histology of sacral DRG from same experiment. Lighter pink region at bottom is ventral root (VR), which does not contain sensory cell bodies for recording. Electrode sites with observed activity are highlighted in yellow, rest are gray. Horizontal position of array does not indicate horizontal movement.

there appeared to be a greater count of clusters closer to the ventral part of the DRG. Other array positions across our experiments did not have a clear trend. The average waveform peak-to-peak amplitude for each electrode site across these array positions is shown in Figure 4 (b). Visually, there was a greater number of mean waveforms above 100 µV peak-to-peak closer to the ventral part of the DRG in this data, aligning with the greater number of clusters observed in these electrode placements. The inconsistent nature of per-electrode site neural activity within and across experiments prevented statistical analyses of any trends. Across other experiment array placements, no clear signal amplitude relationships were observed.

In the same experiment, we recorded neural activity during retraction of the array between positions, while simultaneously brushing the right side of the scrotum. While noise was too high to discern neural activity during the retraction from position 1 to 2, neural activity was recorded from position 2 to 3. Figure 5 shows putative movement of 8 units throughout the retraction. We observed that the movement of recorded units on the array (~600 µm) does not precisely align with the movement of the array itself calculated from the

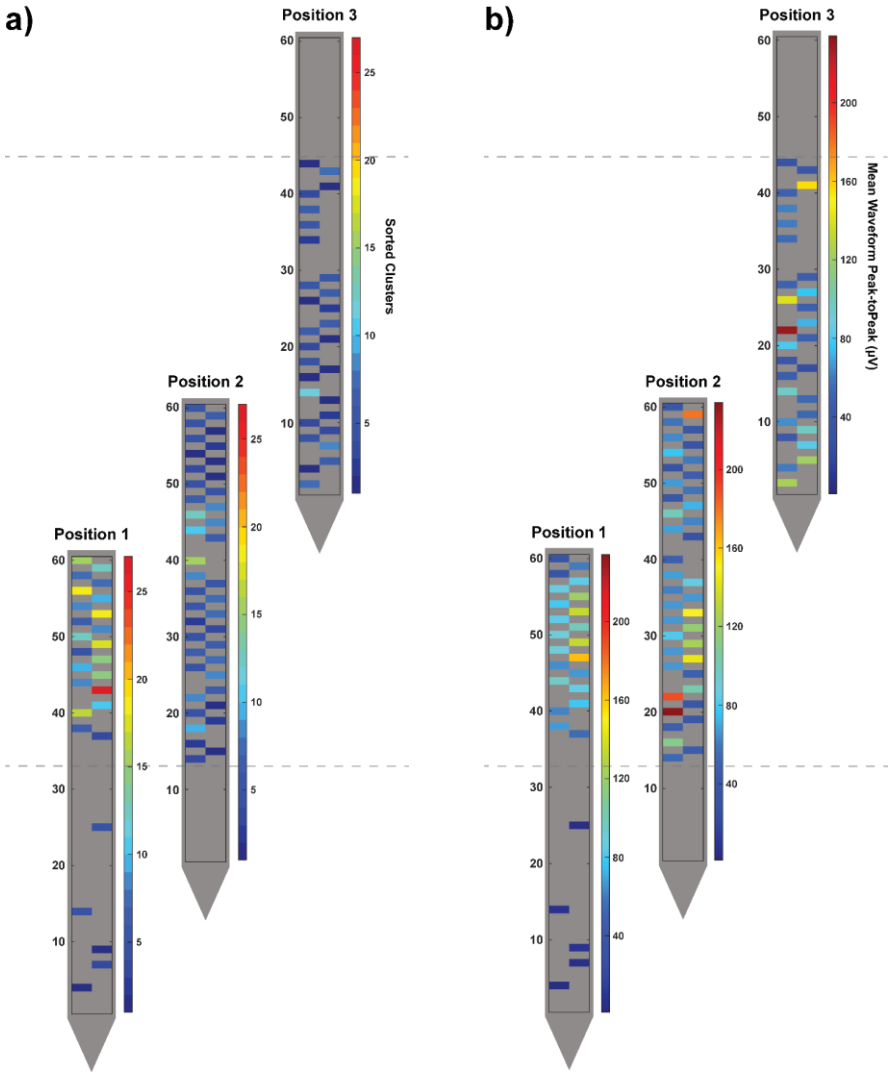

Figure 4: Quantifying observed neural activity across the span of a DRG. a) The number of sorted clusters detected at each electrode site and b) the mean waveform peak-to-peak amplitude at each electrode site are both shown for the three electrode positions in Figure 3. The dotted lines mark the top and bottom of the approximate DRG region where most recordings are expected, per Figure 3.

retraction steps (~960 µm). This is likely a result of slack in the flexible array ribbon. At certain array positions we observed that clusters would shift among electrode sites in a periodic manner, covering a distance on the array of 10-20 µm. This effect is investigated in Figure 6, for the experimental recording session when the array was retracted in steps (Figure 5). Upon closer inspection we determined that the periodic shifting of the recordings generally cycled at a rate which matched the respiration interval (15 breaths per minute = 1 cycle every 4 seconds). For the blue cluster after 150 s and after 200 s in this sequence, there were non-functioning electrode sites within the vertical span that the cluster covered. This led to gaps within the plotting of cluster locations over time shown within Figure 6. As shown in Table 1, we attempted insertion of arrays in 6 different feline experiments. In

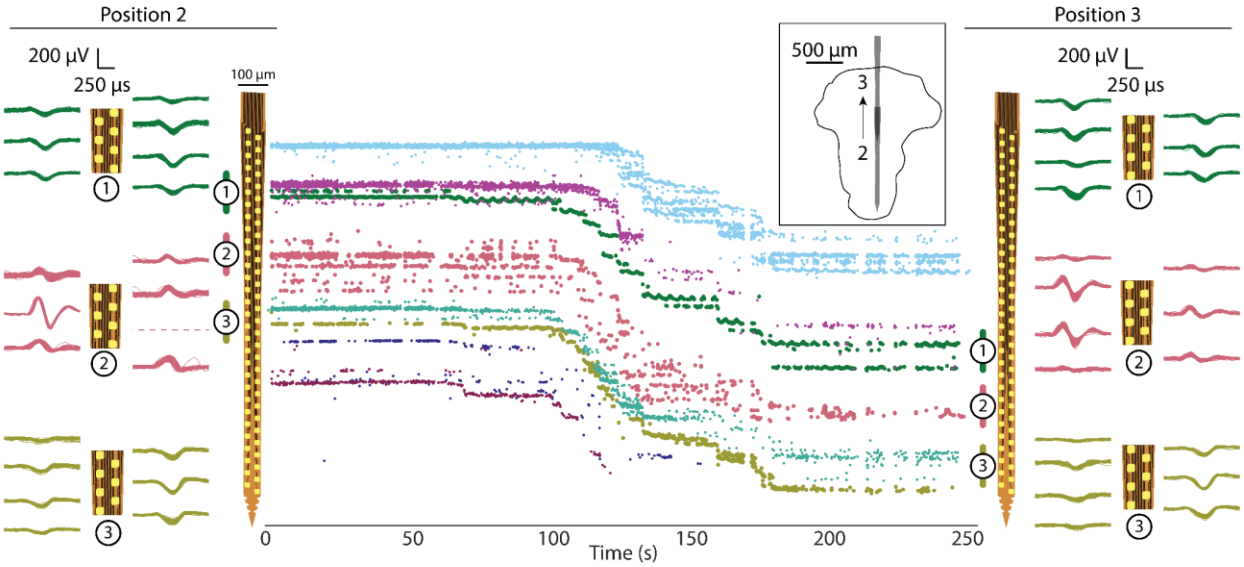

Figure 5: Units tracked across array during withdrawal from position 2 to position 3 (see Figure 3 and inset). As array is withdrawn from DRG, units move relative to the array (toward the tip). Eight units are shown, with movement of approximately 500-600 µm. Waveforms of several of these units are shown at position 2 (left) and position 3 (right) to show similarity of shape.

experiment 6, successful insertion of the array was not achieved. The PEG adhesive used to temporarily adhere the array to the shuttle dissolves quickly. The region around the DRG often had fluid which regularly shifted with breathing. In the first experiment, touching the array to fluid prior to insertion could not be avoided, and the array would not stay adhered for insertion in 2 of 3 insertion attempts. As the temporary adhesion of the array to the shuttle was only briefly successful in experiment 1 and our primary goal in these experiments was to examine DRG mapping capabilities with the array, we subsequently moved to using cyanoacrylate to bond the array to the shuttle for insertion. In experiment 5, while insertion of the array was achieved, no neural activity was observed.

In experiment 6, DRG and system movement due to breathing could not be sufficiently eliminated to allow for clean insertion. Impedance of functional electrodes (<1 MΩ; 47 ± 16 channels in 4 neuron-recording experiments) had a median of 142 kΩ (IQ: 364.3 kΩ) when implanted.

Discussion

In this study we demonstrated acute high-density recordings from feline sacral DRG. This study is the first to measure neural signals from inside DRG with flexible recording arrays and sets a new milestone for recording density in the peripheral nervous system. Using a

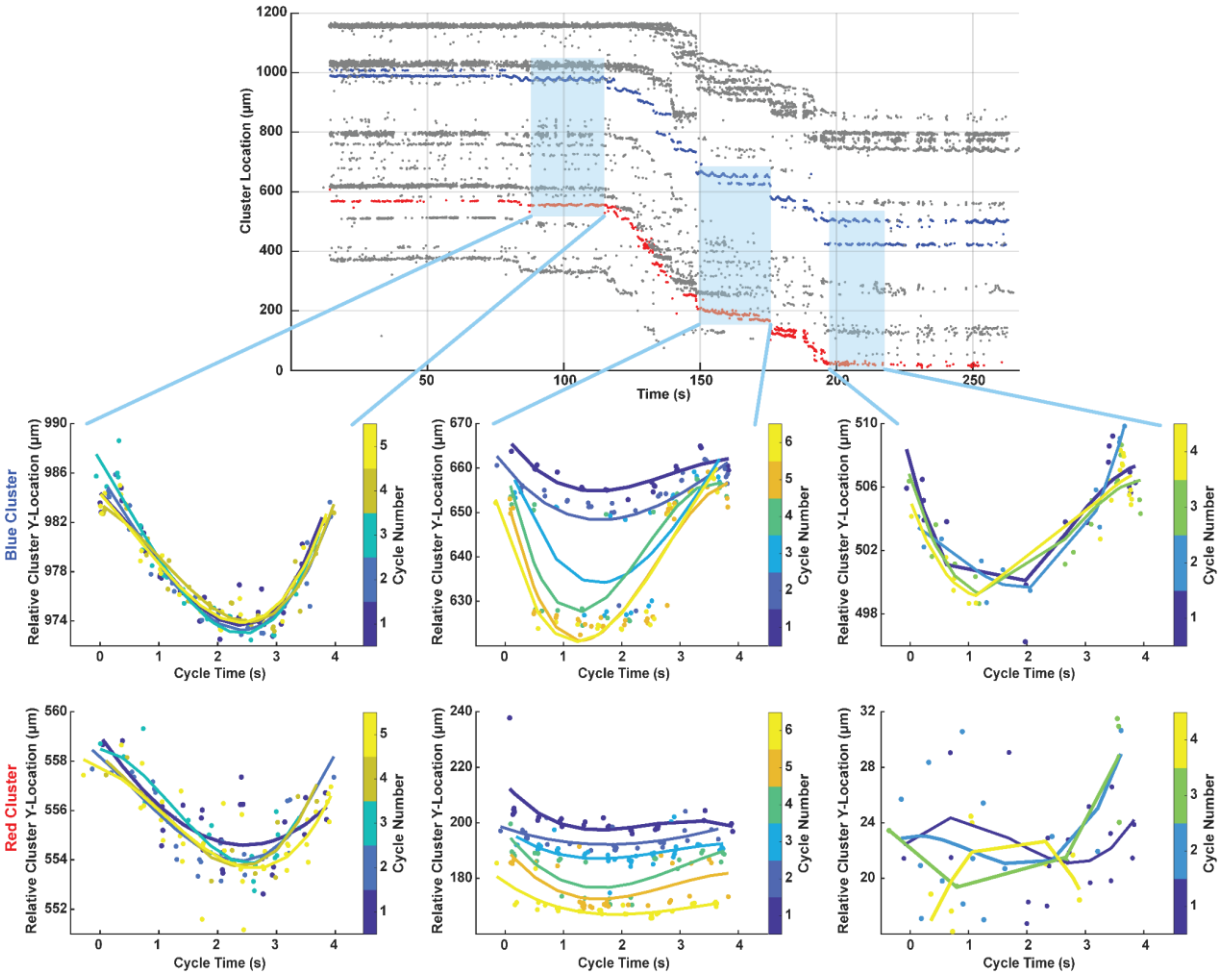

Figure 6: Analysis of breathing effect on clusters shifting among electrode sites, for array movement from position 2 to 3 in Figure 5. Relative vertical locations for two clusters (blue and red in upper plot) are overlaid at four-second intervals per the breathing cycle period for three fixed array locations (light blue shading), showing in some cases a consistent effect on neural recordings. Overlaid on individual data points for each cluster interval cycle is a fit line created with the MATLAB polyfit function. Data points and fit lines are colored per the cycle number key for each sub-plot.

specialized software for sorting high-density neural recordings, we showed that the array was capable of recording neural signals related to bladder pressure and cutaneous brushing in the sacral dermatome, as well as neurons which fire in response to electrical stimulation of the pudendal nerve or anal sphincter. We recorded neural units with peak amplitudes ranging from 20 µV to 1334 µV. Also, we were able to track neural units while the array was physically moved, by using the specialized software that took advantage of the closely-spaced electrode sites. This work shows the potential for high-fidelity interfaces with DRG that can yield new mapping information while being unaffected by relative changes in neuron vertical positions with respect to the array.

A variety of other high-density or special-geometry microelectrodes have been developed for use in the brain [27]. Our work here is an extension of those studies to DRG, examining an over-sampling of local signals to obtain a greater resolution of underlying neural activity. With our high-density probe, we showed that recordings of single units could be achieved on multiple sites for a variety of afferents (Figure 2) and tracked using specialized software as the array moved over ~1 mm (Figure 5). Units which appeared only on a single channel here would have only a ~15% chance of being recorded with a 400 µm pitch Utah array. One recent technology for high-density recording in the brain is the Neuropixels probe, originally reported by Jun et al. (2017) [28]. This is a stiff silicon electrode array with 960 sites spaced at 20 µm. The array has been demonstrated for high-density single-unit recording in the brains of both head-fixed and chronic freely-behaving mice [28], [29]. While the challenges of implanting, fixing, and recording in DRG are very different from brain, the data processing goals and requirements can be very similar. In fact, the same software suite utilized in our study was also utilized in Jun et al. for faster-than-real-time processing on their very high channel count probes [28].

This study is the also first demonstration of high-density recording at this scale in DRG (40 µm site spacing), and one of very few in the peripheral neural system. Previously, the highest density recordings inside DRG used Utah arrays with site spacing of 400 µm [6], [10], [30], [31], except for a single study with 50 µm-spaced electrodes and no report of unit oversampling [16]. While the types of units recorded from sacral DRG in some of these studies were similar (cutaneous, bladder-related, pudendal-stimulation driven), there was no evidence of unit oversampling on neighboring sites. Higher density recordings have been made from the surface of DRG, down to 25 µm electrode site pitch, [19]–[22], but despite the potential advantages of non-penetrating arrays these were fundamentally limited to recording single-unit activity from the shallowest ~150 µm of the DRG [19]. Slightly higher-density recordings have been reported in the peripheral nervous system. For example, 200 µm pitch Utah arrays have been used to record from the sciatic nerve of rats and the pudendal nerve of cats [32], [33]. Transverse intrafascicular multichannel electrodes (TIME), which penetrate across the nerve axis and could hypothetically be used in DRG, have achieved peripheral nerve recordings with sites spaced at ~230 µm [34]. The recordings achieved in our study therefore set a new milestone for recording density in DRG and the peripheral nervous system.

This study, in conjunction with a report focused on the insertion shuttle technology [25], is the first demonstration of flexible bioelectronics delivered into DRG for neural interfacing. Even in an acute experiment, this approach has potential benefits over the standard Utah array, in potentially reducing bleeding or damage from impact of the pneumatic insertion required for Utah array implant [35]–[37]. In chronic experiments, the mechanical mismatch between stiff materials and soft tissue is expected to result in tissue encapsulation of the shank tip, killing or pushing away neurons in the immediate 40-150 µm vicinity [36], [38], [39]. Our chosen delivery method, the small but stiff diamond shuttle with T-shaped profile, was selected based on the unique challenges of delivering a flexible electrode into DRG through the epineurium. In brain implants, flexible probes can utilize less stiff shuttles because the tough dura mater is typically removed in part prior to insertion for animal models larger than a mouse, exposing the significantly softer parenchyma below [40]. In DRG, however, the tough layer of epineurium cannot be easily removed without damage to the underlying neural tissue. Our UNCD shuttle, with its stiffened T-profile, addresses the need for high stiffness this while maintaining a minimal footprint that reduces damage to underlying tissue and blood vessels [25].

The primary analysis suite used in this study, Ironclust, is an open-source MATLAB package specifically designed to take advantage of neural unit oversampling to increase the speed and accuracy of spike sorting [41], [42]. While no specific comparison between manual spike sorting was made in this study, a few general observations can be made from the authors' prior experience with commercial spike sorting software. By considering units identified on clusters of channels, the software saved the effort of separating the same unit on several channels, which was a large time saving. It also mostly eliminated the danger of yield overestimation. One major benefit for those comfortable with coding (the suite is available in a variety of code languages) was the ability to add features and analysis platforms as needed for a particular study. For example, because of this study's focus on unit drift, we added a platform to split units not only in principal component space but also based on spatial center. The open-source nature of the project meant that we were able to integrate useful features into the publicly available package which are now available to other researchers.

There was not a consistent clear trend of high cluster count or high signal amplitude near the DRG edge across experiments. Figure 5 suggests a possible increase in detected

large-amplitude signals towards the ventral aspect of the DRG within that experiment. Prior work by our group has shown that cell bodies are packed around the DRG perimeter [23], [24], which may yield regions with larger signal amplitude recordings. In our experiments here we may not have been activating all neurons within a region. Additionally, some electrode sites may have been close to active axon nodes, which would cause a lower number of individual clusters to be observed. We were not able to estimate source sizes based on the span of array sites that a cluster appeared on, as our recording array was fixed in a two-dimensions and prevented source localization that we accomplished previously with a flexible array on the curved DRG surface [19]. A better understanding of the types of extracellular waveforms that can be recorded near DRG cell bodies, stem axons, and peripheral axons, through computational modeling, may give more insight into the types of neural elements detected in our recordings.

Loss of signal for chronic intraneural experiments is a common problem [10], [36]. We have observed signal loss or signals reappearing over time with single-site electrode shanks chronically implanted in DRG [10]. This may be due to micromotion of the array, scar tissue development, and/or changing of tissue encapsulation over time. The novel array used in this study could mitigate that effect given its small dimensions and flexibility but needs further evidence. We tracked clusters as the electrode was intentionally pulled rostrally 100s of microns (Figure 5). Furthermore, the high density of our array and the IronClust algorithm allowed for clusters to continually be tracked during small changes in electrode site location. In our case, the relative micromotion of the DRG with respect to the array due to breathing led to visible shifts in cluster locations that were easily tracked across the array (Figure 6). We expect that our combination of a high-density flexible interface with the use of the advanced sorting algorithm for unit tracking will allow for a greater long-term signal yield during chronic *in vivo* studies.

This study, while a successful demonstration of high-density flexible penetrating arrays in DRG, also highlighted some important challenges for future studies, especially any that would proceed to chronic implant and recording. The deployment system was designed to temporarily adhere the array to the shuttle with a dissolvable PEG adhesive during insertion followed by removal of the intact shuttle immediately following array release. Supplemental Video 1 shows a successful deployment of the array *in vivo* to the right S2 DRG in experiment 2. In practice, however, fluid in the surgical cavity could wet the adhesive and

cause the array to peel away from the shuttle before insertion. While the system achieved successful delivery in experiment 1, all successful deliveries in following experiments were achieved with permanent cyanoacrylate adhesive to avoid inadvertent early wetting. While we [25] and others [43] demonstrated PEG in rodents, a shuttle inserted through the electrode tip similar to Luan [44] may be more reliable in feline experiments. A future design could use an array with a small loop at the tip to go over the shuttle, which would drive in the array even if the adhesive started to dissolve. The stylet approach has a long history and recently demonstrated on a microscale in the so-called "neural sewing machine" [45].

Another issue with our approach was that, due to large breathing motions following insertion, we not able to successfully withdraw the shuttle without breakage prior to the use of cyanoacrylate. These motions are visible in Supplementary Video 1. We attempted to address this by briefly suspending the breathing cycle during array deployment, but there was insufficient time for the array to fully release from the shuttle before breathing needed to resume. Since the lack of stiff materials in the DRG is one of the primary advantages of our flexible electrodes for chronic use, this issue would need to be solved prior to a long-term implant. One possibility would be to design the shuttle with a controlled breakage point to allow for removal with forceps after the array is securely in place. The natural breakage point of the current shuttle was flush with the DRG surface, making removal difficult. Alternatively, larger "barbs" fabricated as part of the array [46] could hold the array in place during shuttle withdrawal, allowing the shuttle to be removed more quickly.

Assuming these key issues can be addressed, a future chronic study with parallel implant of Utah arrays would be needed to demonstrate the comparative advantage of this technology in both recording longevity and biological response as determined through histological analyses. Continuous neural recording during awake behavior would demonstrate whether the unit tracking demonstrated in this study during array movement would be feasible long-term. This would be a useful feature in developing stable neural decoding for closed-loop neuroprosthesis research. A previous chronic feline study with Utah arrays demonstrated tracking of a bladder DRG neuron over the course of 23 days [10], and computational algorithms can decode bladder pressure from neural firing of one or several units [2], [3], but the long-term stability of these algorithms depends on the ability to monitor multiple bladder neurons over a long period.

While only single arrays were implanted in this study, broader mapping of DRG afferents would require multiple arrays implanted in parallel. This could mean a single device with multiple shanks and/or multiple devices implanted next to each other. Further, this penetrating array could be used in conjunction with previously demonstrated surface arrays [19]. To simplify the implant process, it is possible to envision a combined penetrating-surface interface that would unfold onto the DRG surface during insertion. A similar approach has been previously demonstrated for chronic brain recording in a rat model [39]. This approach could provide an anchor for the surface array, a challenge discussed in our previous study [19].

Conclusions

This study was the first to demonstrate the use of flexible microelectrode arrays to record from within DRG, and to our knowledge the highest-density electrode array reported for use in the DRG or peripheral nervous system. In this study, we recorded a variety of cutaneous, bladder, and electrical-stimulus-driven neural signals from feline sacral DRG in acute anesthetized experiments. We used the high-density data along with specialized open-source software to detect individual neurons recorded on clusters of channels, and to track the "movement" of neural units as an array was slowly withdrawn from the DRG. In the future, we will use these arrays to monitor neurons long-term in awake behavioral studies as we continue to drive the development of neuroprosthetic systems for individuals with neural injury and disease.

Acknowledgements

We acknowledge all members of Dr. Bruns' Peripheral Neural Engineering and Urodynamics Laboratory and Dr. Yoon's Solid-State Electronics Laboratory for valuable assistance in experiments and technology development, especially Aileen Ouyang, Dr. Ahmad Jiman, and Dr. Lauren Zimmerman. Dr. Paras Patel and Elissa Welle assisted in technical aspects of PEDOT coating electrodes. Dr. Mihaly Voroslakos assisted in the design of the array delivery system. Arrays and shuttles were manufactured in the Lurie Nanofabrication Facility at the University of Michigan. Funding for the project was provided by the following: the University of Michigan MiBrain Initiative; the University of Michigan Rackham Predoctoral Fellowship Program; the National Institutes of Health (SPARC awards

U18EB021760 and OT2OD023873, and grant 5R21EB020811); the National Science Foundation (Grant # 1653080).

Author Contributions

Planned study – Z.J.S., K.N., E.Y., J.P.S., T.M.B. Fabricated arrays and shuttles – K.N., J.P.S. Performed surgeries and collected data – Z.J.S., T.M.B. Developed software analysis – Z.J.S., J.J. Analyzed data – Z.J.S., L.R.M., A.S. Drafted manuscript – Z.J.S., L.R.M., T.M.B. Reviewed manuscript and approved final version – Z.J.S., K.N., L.R.M., A.S., E.Y., J.J., J.P.S., T.M.B. Supervised project – E.Y., J.P.S., T.M.B.

Data Availability Statement

The raw neural and analog recording data that support the findings of this study and will be available with associated metadata from the Blackfynn Discovery platform at doi: 10.26275/vzxw-kwdu after curation by the NIH SPARC Data Resource Center. This includes all data used to generate Figures 2-6, as well as summary data.

Code Availability Statement

All analysis in this study was performed using ironclust, a neural spike sorting package for MATLAB developed at Flatiron Institute, based on JRCLUST (Janelia Rocket Cluster). The current version of this software, which includes features developed for this study, can be found at https://github.com/flatironinstitute/ironclust.

Competing Interests

T.M.B. is a named inventor on a granted patent (US9622671B2; assigned to University of Pittsburgh) which is on the monitoring of physiological states via microelectrodes at DRG. The authors declare no other personal or institutional interest with regards to the authorship and/or publication of this manuscript.

References

[1] Y. Aoyagi, R. B. Stein, A. Branner, K. G. Pearson, and R. A. Normann, “Capabilities of a penetrating microelectrode array for recording single units in dorsal root ganglia of the cat,” *J. Neurosci. Methods*, vol. 128, pp. 9–20, 2003.

[2] S. E. Ross, Z. Ouyang, S. Rajagopalan, and T. M. Bruns, "Evaluation of Decoding Algorithms for Estimating Bladder Pressure from Dorsal Root Ganglia Neural Recordings," *Ann. Biomed. Eng.*, vol. 46, no. 2, pp. 233–246, Feb. 2018.

[3] Z. Ouyang, Z. J. Sperry, N. D. Barrera, and T. M. Bruns, "Real-time Bladder Pressure Estimation for Closed-loop Control in a Detrusor Overactivity Model," *IEEE Trans. Neural Syst. Rehabil. Eng.*, vol. 27, no. 6, pp. 1209–1216, 2019.

[4] R. B. Stein *et al.*, "Coding of position by simultaneously recorded sensory neurones in the cat dorsal root ganglion.," *J. Physiol.*, vol. 560, no. 3, pp. 883–896, 2004.

[5] B. J. Holinski, D. G. Everaert, V. K. Mushahwar, and R. B. Stein, "Real-time control of walking using recordings from dorsal root ganglia.," *J. Neural Eng.*, vol. 10, no. 5, p. 056008, 2013.

[6] D. J. Weber, R. B. Stein, D. G. Everaert, and A. Prochazka, "Limb-state feedback from ensembles of simultaneously recorded dorsal root ganglion neurons.," *J. Neural Eng.*, vol. 4, no. 3, pp. S168–S180, 2007.

[7] J. Rigosa, D. J. Weber, A. Prochazka, R. B. Stein, and S. Micera, "Neuro-fuzzy decoding of sensory information from ensembles of simultaneously recorded dorsal root ganglion neurons for functional electrical stimulation applications," *J. Neural Eng.*, vol. 8, no. 4, p. 046019, 2011.

[8] W. J. T. Wessels, H. K. P. Feirabend, and E. Marani, "Evidence for a rostrocaudal organization in dorsal root ganglia during development as demonstrated by intra-uterine WGA-HRP injections into the hindlimb of rat fetuses," *Dev. Brain Res.*, vol. 54, no. 2, pp. 273–281, 1990.

[9] W. J. T. Wessels, H. K. P. Feirabend, and E. Marani, "Somatotopic organization in the sensory innervation of the rat hindlimb during development, using half dorsal root ganglia as subsegmental units.," *Eur. J. Morphol.*, vol. 28, no. 2–4, pp. 394–403, 1990.

[10] A. Khurram *et al.*, "Chronic monitoring of lower urinary tract activity via a sacral dorsal root ganglia interface," *J. Neural Eng.*, vol. 14, no. 3, p. 036027, 2017.

[11] L. E. Fisher, C. A. Ayers, M. Ciollaro, V. Ventura, D. J. Weber, and R. A. Gaunt, "Chronic recruitment of primary afferent neurons by microstimulation in the feline dorsal root ganglia," *J. Neural Eng.*, vol. 11, no. 3, p. 036007, 2014.

[12] C. A. Ayers, L. E. Fisher, R. A. Gaunt, and D. J. Weber, "Microstimulation of the lumbar DRG recruits primary afferent neurons in localized regions of lower limb," *J.*

Neurophysiol., vol. 116, no. 1, pp. 51–60, 2016.

[13] A. C. Nanivadekar, C. A. Ayers, R. A. Gaunt, D. J. Weber, and L. E. Fisher, "Selectivity of afferent microstimulation at the DRG using epineural and penetrating electrode arrays," *J. Neural Eng.*, vol. 17, no. 1, 2020.

[14] K. W. King *et al.*, "DRG microstimulation evokes postural responses in awake, standing felines," *J. Neural Eng.*, vol. 17, no. 1, 2020.

[15] C. L. Kolarcik *et al.*, "Host tissue response to floating microelectrode arrays chronically implanted in the feline spinal nerve," *J. Neural Eng.*, vol. 17, no. 4, p. 046012, Jul. 2020.

[16] A. E. Snellings, P. B. Yoo, and W. M. Grill, "Urethral flow-responsive afferents in the cat sacral dorsal root ganglia.," *Neurosci. Lett.*, vol. 516, no. 1, pp. 34–38, 2012.

[17] G. C. McConnell, H. D. Rees, A. I. Levey, C. A. Gutekunst, R. E. Gross, and R. V. Bellamkonda, "Implanted neural electrodes cause chronic, local inflammation that is correlated with local neurodegeneration," *J. Neural Eng.*, vol. 6, no. 5, 2009.

[18] P. J. Rousche, D. S. Pellinen, D. P. Pivin, J. C. Williams, R. J. Vetter, and D. R. Kipke, "Flexible polyimide-based intracortical electrode arrays with bioactive capability," *IEEE Trans. Biomed. Eng.*, vol. 48, no. 3, pp. 361–371, 2001.

[19] Z. J. Sperry *et al.*, "Flexible microelectrode array for interfacing with the surface of neural ganglia," *J. Neural Eng.*, vol. 15, no. 3, p. 036027, 2018.

[20] R. A. Gaunt, T. M. Bruns, D. J. Crammond, N. D. Tomycz, J. J. Moossy, and D. J. Weber, "Single- and multi-unit activity recorded from the surface of the dorsal root ganglia with non-penetrating electrode arrays," *Proc. Annu. Int. Conf. IEEE Eng. Med. Biol. Soc. EMBS*, pp. 6713–6716, 2011.

[21] A. I. Kashkoush, R. A. Gaunt, L. E. Fisher, T. M. Bruns, and D. J. Weber, "Recording single- and multi-unit neuronal action potentials from the surface of the dorsal root ganglion," *Sci. Rep.*, vol. 9, no. 1, p. 2786, 2019.

[22] W.-C. Huang *et al.*, "Ultracompliant Hydrogel-Based Neural Interfaces Fabricated by Aqueous-Phase Microtransfer Printing," *Adv. Funct. Mater.*, p. 1801059, 2018.

[23] A. K. Ostrowski, Z. J. Sperry, G. Kulik, and T. M. Bruns, "Quantitative models of feline lumbosacral dorsal root ganglia cell density," *Neurosci. Methods*, vol. 290, pp. 116–124, 2017.

[24] Z. J. Sperry, R. D. Graham, N. Peck-Dimit, S. F. Lempka, and T. M. Bruns, "Spatial

models of cell distribution in human lumbar dorsal root ganglia," *J. Comp. Neurol.*, vol. 528, pp. 1644–1659, 2020.

[25] K. Na *et al.*, "Novel diamond shuttle to deliver flexible bioelectronics with reduced tissue compression," *Microsystems Nanoeng.*, vol. 6 p. 37, 2020.

[26] E. P. Gardner and K. O. Johnson, "The Somatosensory System: Receptors and Central Pathways," in *Principles of Neural Science, Fifth Edition*, New York, NY: McGraw-Hill Education, 2014.

[27] J. P. Seymour, F. Wu, K. D. Wise, and E. Yoon, "State-of-the-art MEMS and microsystem tools for brain research," *Microsystems Nanoeng.*, vol. 3, no. March 2016, pp. 1–16, 2017.

[28] J. J. Jun *et al.*, "Fully integrated silicon probes for high-density recording of neural activity," *Nature*, vol. 551, no. 7679, pp. 232–236, 2017.

[29] A. Juavinett, G. Bekheet, and A. Churchland, "Chronically-implanted Neuropixels probes enable high yield recordings in freely moving mice," *Elife*, vol. 8, p. e47188, 2019.

[30] T. M. Bruns, R. A. Gaunt, and D. J. Weber, "Multielectrode array recordings of bladder and perineal primary afferent activity from the sacral dorsal root ganglia," *J. Neural Eng.*, vol. 8, no. 5, p. 056010, Oct. 2011.

[31] D. J. Weber, R. B. Stein, D. G. Everaert, and A. Prochazka, "Decoding sensory feedback from firing rates of afferent ensembles recorded in cat dorsal root ganglia in normal locomotion," *IEEE Trans. Neural Syst. Rehabil. Eng.*, vol. 14, no. 2, pp. 240–243, 2006.

[32] H. A. C. C. Wark *et al.*, "A new high-density (25 electrodes/mm2) penetrating microelectrode array for recording and stimulating sub-millimeter neuroanatomical structures," *J. Neural Eng.*, vol. 10, no. 4, p. 045003, 2013.

[33] K. S. Mathews *et al.*, "Acute monitoring of genitourinary function using intrafascicular electrodes: selective pudendal nerve activity corresponding to bladder filling, bladder fullness, and genital stimulation.," *Urology*, vol. 84, no. 3, pp. 722–9, Sep. 2014.

[34] T. Boretius *et al.*, "A transverse intrafascicular multichannel electrode (TIME) to interface with the peripheral nerve.," *Biosens. Bioelectron.*, vol. 26, no. 1, pp. 62–69, Sep. 2010.

[35] P. J. Rousche and R. A. Normann, "A method for pneumatically inserting an array of penetrating electrodes into cortical tissue," *Ann. Biomed. Eng.*, vol. 20, no. 4, pp. 413–

422, 1992.

[36] A. Branner, R. B. Stein, E. Fernandez, Y. Aoyagi, and R. A. Normann, "Long-Term Stimulation and Recording with a Penetrating Microelectrode Array in Cat Sciatic Nerve," *IEEE Trans. Biomed. Eng.*, vol. 51, no. 1, pp. 146–157, 2004.

[37] M. B. Christensen, S. M. Pearce, N. M. Ledbetter, D. J. Warren, G. A. Clark, and P. A. Tresco, "The foreign body response to the Utah Slant Electrode Array in the cat sciatic nerve," *Acta Biomater.*, vol. 10, no. 11, pp. 4650–4660, 2014.

[38] H. A. C. Wark, K. S. Mathews, R. A. Normann, and E. Fernandez, "Behavioral and cellular consequences of high-electrode count Utah Arrays chronically implanted in rat sciatic nerve.," *J. Neural Eng.*, vol. 11, no. 4, p. 046027, 2014.

[39] D. McCreery, S. Cogan, S. Kane, and V. Pikov, "Correlations between histology and neuronal activity recorded by microelectrodes implanted chronically in the cerebral cortex," *J. Neural Eng.*, vol. 13, no. 3, p. 036012, 2016.

[40] T. D. Y. Kozai *et al.*, "Reduction of neurovascular damage resulting from microelectrode insertion into the cerebral cortex using in vivo two-photon mapping," *J. Neural Eng.*, vol. 7, no. 4, p. 046011, 2010.

[41] J. J. Jun, C. Mitelut, C. Lai, S. L. Gratiy, C. A. Anastassiou, and T. D. Harris, "Real-time spike sorting platform for high-density extracellular probes with ground-truth validation and drift correction," *bioRxiv*, p. 101030, 2017.

[42] J. Magland *et al.*, "SpikeForest, reproducible web-facing ground-truth validation of automated neural spike sorters," *Elife*, vol. 9, p. 2020.01.14.900688, May 2020.

[43] T. Suzuki, K. Mabuchi, and S. Takeuchi, "A 3D flexible parylene probe array for multichannel neural recording," in *First International IEEE EMBS Conference on Neural Engineering, 2003. Conference Proceedings.*, 2003, pp. 154–156.

[44] L. Luan *et al.*, "Ultraflexible nanoelectronic probes form reliable, glial scar–free neural integration," *Sci. Adv.*, vol. 3, no. 2, p. e1601966, 2017.

[45] T. L. Hanson, C. A. Diaz-Botia, V. Kharazia, M. M. Maharbiz, and P. N. Sabes, "The 'sewing machine' for minimally invasive neural recording," *bioRxiv*, p. 578542, 2019.

[46] V. Gaillet *et al.*, "Spatially selective activation of the visual cortex via intraneural stimulation of the optic nerve," *Nat. Biomed. Eng.*, 2019.

[47] P. R. Patel *et al.*, "Chronic in vivo stability assessment of carbon fiber microelectrode arrays," *J. Neural Eng.*, vol. 13, no. 6, p. 066002, Dec. 2016.

[48] R. A. Kuhn, "Organization of Tactile Dermatomes in Cat and Monkey," *J. Neurophysiol.*, vol. 16, pp. 169–182, 1952.

[49] R. Q. Quiroga, Z. Nadasdy, and Y. Ben-Shaul, "Unsupervised Spike Detection and Sorting with Wavelets and Superparamagnetic Clustering," *Neural Comput.*, vol. 16, no. 8, pp. 1661–1687, 2004.

[50] A. Rodriguez and A. Laio, "Clustering by fast search and find of density peaks," *Science (80-.).*, vol. 344, no. 6191, pp. 1492–1496, 2014.

[51] A. Rodriguez, M. D'Errico, E. Facco, and A. Laio, "Computing the Free Energy without Collective Variables," *J. Chem. Theory Comput.*, vol. 14, no. 3, pp. 1206–1215, 2018.